ISSN 1003-501X CN 51-1346/O4

光电工程

Opto-Electronic Engineering

中文核心期刊 中国科技核心期刊

Scopus CSCD

星载望远镜消光材料积分散射特性测试研究(英文)

刘巍，李朝辉，毛振，赵建科，朱辉，魏紫薇，刘勇，尹云飞

引用本文:

刘巍，李朝辉，毛振，等. 星载望远镜消光材料积分散射特性测试研究(英文)[J]. 光电工程，2024， **51**(2): 230206.

Liu W, Li Z H, Mao Z, et al. Research on integrated scattering characteristics of extinctive materials for spaceborne telescopes[J]. *Opto-Electron Eng*, 2024, **51**(2): 230206.

https://doi.org/10.12086/oee.2024.230206

收稿日期: 2023-08-24; 修改日期: 2024-01-11; 录用日期: 2024-01-11

相关论文

空间引力波探测望远镜研究进展

王小勇，白绍竣，张倩，林栩凌，李洋，夏晨晖

光电工程 2023, **50**(11): 230219 doi: 10.12086/oee.2023.230219

空间引力波探测系统中超光滑光学元件表面散射特性分析

张耘豪，钟哲强，张彬

光电工程 2023, **50**(11): 230222 doi: 10.12086/oee.2023.230222

空间引力波星载望远镜测试与评估技术研究进展

张兰强，曾意，吴小虎，杨金生，阮晓莉，辛强，顾乃庭，饶长辉

光电工程 2024, **51**(2): 240027 doi: 10.12086/oee.2024.240027

基于强化学习的空间引力波探测望远镜系统外杂光抑制研究

张梓扬，常军，黄一帆，陈钦芳，吴郁楠

光电工程 2024, **51**(2): 230210 doi: 10.12086/oee.2024.230210

更多相关论文见光电期刊集群网站

Opto-Electronic Engineering
光 电 工 程

空间引力波探测
星载望远镜专题（二）

Article

2024 年, 第 51 卷, 第 2 期

DOI: 10.12086/oee.2024.230206

星载望远镜消光材料积分散射特性测试研究 (英文)

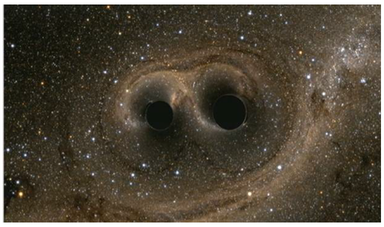

刘 巍[1*]，李朝辉[1]，毛 振[1,2]，赵建科[1]，朱 辉[1]，
魏紫薇[1]，刘 勇[1]，尹云飞[1]

[1]中国科学院西安光学精密机械研究所，陕西 西安 710119；
[2]中国科学院大学，北京 100049

摘要：在散射理论的基础上，介绍了一种星载望远镜消光材料积分散射特性测试装置，实现对星载望远镜消光材料散射特性更为全面的测量。对积分散射理论、系统构造、系统性能进行了阐述。对系统进行建模仿真分析，得到结论：消光材料的散射特性在不同点位和入射角下存在明显差异，系统能够测量多种条件下消光材料的散射特性，并得到消光材料全面的散射特性分布。研究结果为根据消光材料特性进行针对性设计提供了更全面、更准确的散射特性分布，为杂散光的测量与抑制、高性能光学仪器的研制与装调以及计算光学等领域的研究提供了参考。为空间引力波探测星载望远镜系统的材料选型、特性研究、杂散光分析与抑制提供了基础。

关键词：空间引力波探测；星载望远镜；散射分布；高精度测量

中图分类号：TN206　　　　**文献标志码：**A

刘巍，李朝辉，毛振，等. 星载望远镜消光材料积分散射特性测试研究 (英文)[J]. 光电工程，2024，**51**(2): 230206
Liu W, Li Z H, Mao Z, et al. Research on integrated scattering characteristics of extinctive materials for spaceborne telescopes[J]. *Opto-Electron Eng*, 2024, **51**(2): 230206

Research on integrated scattering characteristics of extinctive materials for spaceborne telescopes

Liu Wei[1*], Li Zhaohui[1], Mao Zhen[1,2], Zhao Jianke[1], Zhu Hui[1],
Wei Ziwei[1], Liu Yong[1], Yin Yunfei[1]

[1]Xi'an Institute of Optics and Precision Mechanics, Chinese Academy of Sciences, Xi'an, Shaanxi 710119, China;
[2]University of Chinese Academy of Sciences, Beijing 100049, China

Abstract: This paper presents a novel test device for evaluating the integral scattering characteristics of the extinction material in spaceborne telescopes. By employing the scattering theory, the device enables a more comprehensive measurement of the scattering characteristics, facilitating a better understanding of the material's behavior. The paper discusses in detail the integral scattering theory, system construction, and system performance. The system is further modeled and simulated, leading to the conclusion that the scattering characteristics of the extinction material exhibit significant variations at different points and incident angles. Notably, the system is capable of measuring the scattering characteristics under various conditions, thereby providing a comprehensive distribution of the material's scattering behavior. This comprehensive and accurate scattering characteristic distribution serves as a valuable reference for targeted design, stray light measurement and

收稿日期：2023-08-24；修回日期：2024-01-11；录用日期：2024-01-11
基金项目：国家重点研发计划资助项目 (2021YFC2202203)
*通信作者：刘巍，liuwei1@opt.ac.cn。

suppression, development of high-performance optical instruments, and research in computational optics. Moreover, it establishes a solid foundation for material selection, characteristic investigation, stray light analysis, and suppression in spaceborne telescopes employed for the detection of gravitational waves.

Keywords: gravitational wave detection in space; spaceborne telescope; scattering distribution; high-precision measurement

Introduction

In 2015, the Laser Interferometer Gravitational-Wave Observatory (LIGO) made a groundbreaking discovery by detecting gravitational waves generated from the collision of two black holes. This historic event not only confirmed the existence of gravitational waves but also provided a novel means to observe and understand the universe, as shown in Fig. 1. Since the 21st century, there has been rapid development in science and technology, providing unprecedented opportunities for the advancement of laser gyroscopes, aerospace, geological exploration, space optics, and testing and measurement. Consequently, there is an increasing demand for research and manufacturing of various high-end instruments, leading to a greater urgency for optics and related technologies. It is imperative for optical systems to possess higher and more stable imaging quality.

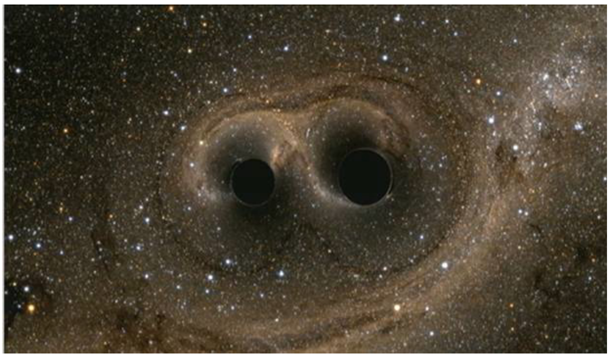

Fig. 1 Gravitational wave detection

Space telescopes play a vital role in modern astronomical research[1]. To obtain accurate and clear astronomical images, the optical systems of telescopes must effectively minimize the interference caused by scattering light from the Earth's atmosphere and other sources, as shown in Fig. 2. To achieve this objective, attenuating materials are widely employed in the optical systems of telescopes.

Fig. 2 Selection of light-absorbing materials

Attenuating materials are characterized by their excellent ability to absorb or scatter scattered light from the light source, thereby reducing interference. However, evaluating and testing the performance of attenuating materials is a complex and crucial task that necessitates an in-depth study of their integral scattering characteristics.

Integral scattering characteristics refer to the materials' ability to scatter incident light, which directly affects the resolution and sensitivity of the telescope system[2]. Thus, accurate testing and research on the integral scattering characteristics of attenuating materials for space telescopes are of utmost importance.

Theoretical analysis

The integral scattering theory is derived from the Rayleigh-Rice[3-4] vector perturbation theory, which explains the relationship between the power density of scattering and the surface power spectral density per unit incident power for smooth surfaces[5-7]:

$$\frac{\mathrm{d}P_{\mathrm{s}}/\mathrm{d}\Omega_{\mathrm{s}}}{P_{\mathrm{i}}}\cdot\mathrm{d}\Omega_{\mathrm{s}}=\left(\frac{16\pi^2}{\lambda^4}\right)\cos\theta_{\mathrm{i}}\cos^2\theta_{\mathrm{s}}QS\left(f_x,f_y\right)\mathrm{d}\Omega_{\mathrm{s}}. \quad (1)$$

The equation is composed of several components. First, Q represents the reflectance, which measures the amount of light or radiation reflected by a surface.

Second, $S(f_x, f_y)$ denotes the power spectral density of the measured surface. This term captures the distribution of power across different spatial frequencies, indicating the surface′s variation and texture. Finally, the expressions for f_x and f_y, representing spatial frequencies, are provided in Eqs. (2) and (3)[8-10].

$$f_x = \frac{\sin\theta_s \cos f_s - \sin\theta_i}{\lambda}, \tag{2}$$

$$f_y = \frac{\sin\theta_s \sin\phi_s}{\lambda}. \tag{3}$$

$\frac{\mathrm{d}P_s/\mathrm{d}\Omega_s}{P_i}\cdot \mathrm{d}\Omega_s$ represents the power density of scattered radiation relative to the incident power. P_i represents the power of incident light, while P_m signifies the power of reflected light. A represents the measured surface, and its normal is parallel to the A axis. Lambda (λ) denotes the wavelength of incident light. θ_i, θ_s and Φ_s represent the incident angle, scattering angle, and scattering azimuth angle, respectively. $\mathrm{d}\Omega_s$ represents the differential solid angle in the s direction, and it is given by $\mathrm{d}\Omega_s = \sin\theta_s \mathrm{d}\phi_s \mathrm{d}\theta_s$. $\mathrm{d}P_s$ is the scattered light power within the solid angle $\mathrm{d}\Omega_s$.

The selection of the coordinate system in the formula is illustrated in Fig. 3 [11-14].

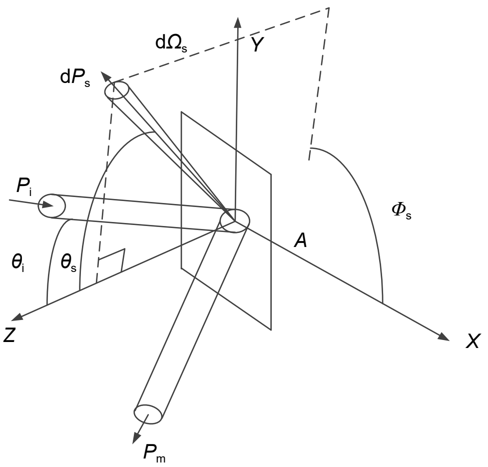

Fig. 3 Scatter plot coordinate system schematic

The total integrated scattering (TIS) is defined as the ratio between the power of scattered light and the power of specular reflected light[15-17].

$$TIS = \frac{P_s}{P_m} = \int_0^{2\pi}\int_{\theta_{\min}}^{\theta_{\max}} \frac{\mathrm{d}P\mathrm{d}\Omega_s}{RP_i}\mathrm{d}\Omega\,. \tag{4}$$

From the Eq. (4) above, we derive:

$$TIS = \left(\frac{4\pi}{\lambda}\right)^2 \iint_f \cos\theta_i \cos\theta_s S(f_x, f_y)\mathrm{d}f_x \mathrm{d}f_y\,. \tag{5}$$

Due to the relationship between surface power spectral density and root mean square roughness:

$$\sigma^2 = \iint_f S(f_x, f_y)\mathrm{d}f_x \mathrm{d}f_y\,. \tag{6}$$

In this study, we aim to enhance the clarity and readability of the article by deriving the total integral scattering TIS through its substitution into Eq. (5). We provide suggestions for improving sentence structure, grammar, word choice, and overall expression to achieve this goal[18-20].

$$\begin{aligned} TIS &= \left(\frac{4\pi}{\lambda}\right)^2 \iint_f \cos\theta_i \cos\theta_s S(f_x, f_y)\mathrm{d}f_x \mathrm{d}f_y \\ &\approx \left(\frac{4\pi n_i \cos\theta_i \sigma}{\lambda}\right)^2. \end{aligned} \tag{7}$$

From Eq. (7), it is evident that the angle of incidence of light and the surface roughness of a component have a considerable impact on its total integrated scattering (TIS). This study aims to investigate the relationship between these factors and TIS by analyzing experimental measurements. The obtained data allow us to establish a correlation between the angle of incidence, surface roughness, and TIS. The findings of this research enhance our understanding of the factors influencing TIS, which is vital for the design and optimization of components in diverse applications.

The scattering characteristic distribution of components is a crucial parameter for describing their scattering phenomenon across different wavelengths[21-22]. It enables a deeper comprehension of the physical properties and behavioral patterns of these components. The precise detection of the multi-dimensional scattering characteristic distribution holds immense significance in diverse scientific research and engineering applications.

System structure

Space-based telescopes have stringent requirements for stray light suppression, necessitating comprehensive measurements of the scattering characteristics of extinction materials. Practical testing usually yields only approximate scattering characteristics of individual components due to factors like the material, processing, and assembly, which fail to represent the comprehensive distribution of scattering characteristics. Conducting comprehensive and high-precision measurements of scattering characteristics is crucial to accurately simulate the operating environment and enhance the specificity and effectiveness of material selection for relevant design purposes.

Based on the principle of scattered light detection, this study examines and investigates the design characteristics of both domestic and international scattered light measurement systems. By integrating existing scattered light measurement devices, a novel multi-element high-precision scattered light distribution measurement system is devised. This system enables accurate and effortless measurement of the scattering characteristics distribution of the test element at different distances.

The multi-dimensional high-precision measurement system for the distribution of component scattering characteristics, illustrated in Fig. 4, is composed of three main components: the light emission unit, the light interaction unit, and the data processing unit. In the light emission unit, a laser emits light that is modulated by an acousto-optic modulator and then directed towards a beamsplitter. One beam serves as a reference signal for Detector 1, while the other beam enters the light interaction unit. The laser and acousto-optic modulator are mounted on an electric rotary stage equipped with an encoder that provides real-time rotation angle data. This setup enables real-time measurement of the incident light angle and allows for continuous variation of incident angles to accurately assess the distribution of stray light within the entire field of view. A high-precision acousto-optic modulator is utilized to shift the signal to a high-frequency range, effectively eliminating low-frequency noise interference from both the system and the environment. Within the light interaction unit, the incident light illuminates the surface of the component under examination. The light directly reflected from the mirror is directed out through an aperture and captured by Detector 2. The scattered light emitted from the component under test is dispersed in multiple directions, reflected within an integrating sphere, and subsequently enters integrating sphere 2. Detector 3 detects the integrated scattered light at the exit port of integrating sphere 2, allowing for the acquisition of scattered light information at different levels. The information processing system analyzes and computes the scattered light data collected by the detectors, enabling the extraction of scattering information from the component. This system offers several advantages over traditional scattering measurement systems, including the ability to measure component scattering distribution in multiple dimensions and enhanced measurement accuracy.

The innovation of this system is based on integral scattering, which is utilized for measuring the scattering characteristics on the surface of components. It offers several advantages such as simplicity in operation, high detection efficiency, and the elimination of complex calibration processes. The component under examination is positioned at the sampling port of integrating sphere *A*, ensuring a non-contact detection process that does not harm the component's surface. Moreover, it does not necessitate the expertise of professional technicians, resulting in cost reduction for testing. The system incorporates a frequency shift modulator positioned behind the light source. This modulator adjusts the frequency of the incident light to meet the requirements and filters out environmental noise interference. Consequently, only the effective light signal passes through, resulting in improved signal-to-noise ratio and enhanced detection accuracy. A beamsplitter is placed after the frequency shift modulator, dividing the modulated light into a reflected light beam that serves as a reference. This reference light signal is then captured by a third detector. Based on the reference light signal, the first and second light signals are denoised, resulting in further improvement in detection accuracy. The light source component of this system is mounted on a turntable, enabling the rotation to change the incident angle of the detection light. This feature allows for multi-angle continuous measurement, enhancing the

 https://doi.org/10.12086/oee.2024.230206

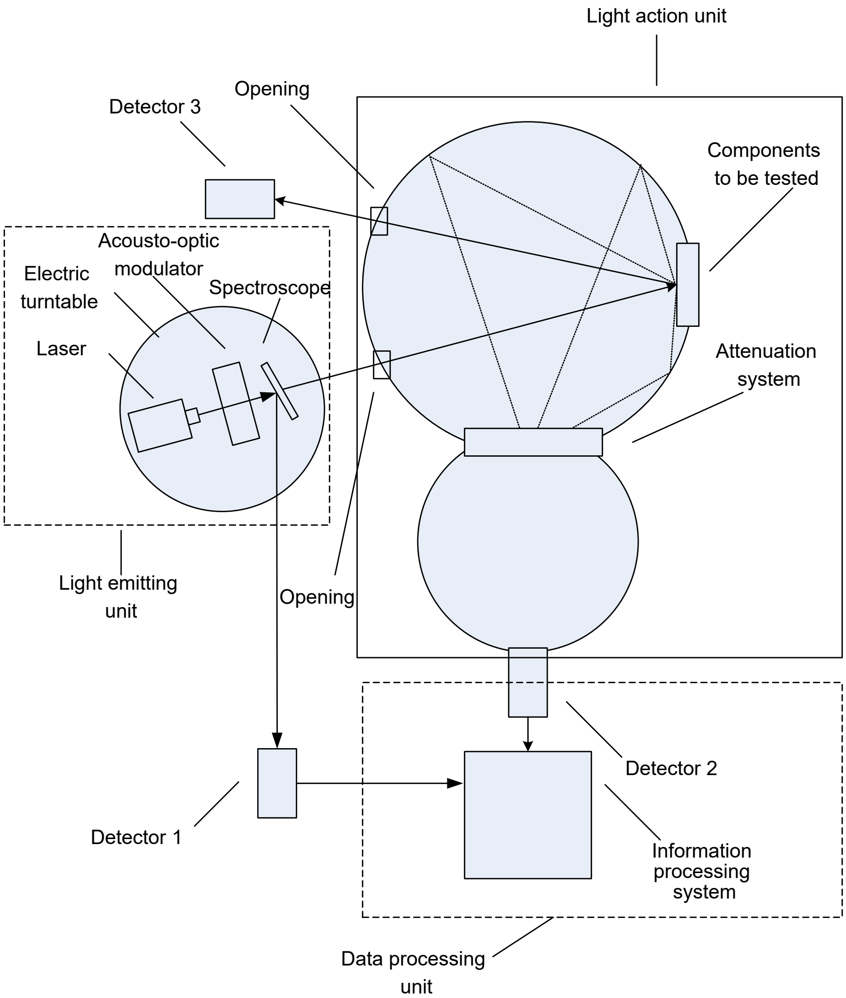

Fig. 4 Multivariate high-precision measurement system for element scattering characteristic distribution

comprehensiveness and precision of detection.

Modeling analysis

The stray light measurement system is used for modeling and conducting full-field stray light analysis of the test component. The results are then compared with those obtained using traditional measurement systems. The integration sphere is modeled by considering its diameter (Φ), opening area (A_0), internal cavity area (A_1), and the diffuse reflectance (ρ) of its internal surface material. When incident light interacts with the sample, it is divided into two parts: the specular part, which reflects off the mirror and exits, and the diffuse reflection part, which scatters multiple times on the internal surface of the integration sphere before reaching the detector's surface. The opening ratio of the integration sphere is defined as the sum of its opening areas divided by the total internal surface area.

$$f = \frac{A_0}{A_1} = \left(\frac{\sum_{\mathrm{i}} \pi \cdot \Phi_{\mathrm{i}}^{2}/4}{4\pi \cdot \Phi^2/4} \right)^2 = 0.67\%. \tag{8}$$

The equation represents an integrating sphere, which consists of an aperture area denoted as A_0 and an internal cavity area denoted as A_1.

The radiation energy remaining within the integral sphere cavity after multiple diffusions is:

$$\phi_{\mathrm{o}} = \sum \phi' = \frac{\rho \phi_{\mathrm{i}}}{1-\rho(1-f)}. \tag{9}$$

The irradiance E at any point inside the sphere of integration is given by:

$$E = \frac{\sum \phi'}{A} = \frac{\rho\phi_{\mathrm{i}}}{A[1-\rho(1-f)]} = \frac{\rho\phi_{\mathrm{i}}}{4\pi R^2[1-\rho(1-f)]}. \tag{10}$$

A is the surface area of the integrating sphere; ρ is the spectral reflectance of the inner wall of the integrating sphere (taken as 0.98); ϕ_i is the total radiant energy incident into the integrating sphere; R is the radius of the sphere inside the integrating sphere.

For a standard white Lambertian panel, the energy received by the detector is:

$$P_R = E \cdot \pi R^2. \tag{11}$$

The absorption rate of SB-3 material is approximately 98%, while the detector receives only about 2% of the energy from the whiteboard.

An integration sphere of Φ300 mm in diameter was constructed. The aperture sizes for incident/reflective, sample, and detector were set at Φ20 mm, Φ40 mm, and Φ0.5 mm, respectively. The incident power was adjusted to 1 W, and the simulation materials employed were SB-3 (aluminum substrate) and a whiteboard. Additionally, the incident beam diameter was specified as Φ4 mm.

Initially, we utilize the SB-3 substance and establish the quantity of beams and energy threshold for ray tracing. The correlation between the number of beams and detector response is displayed in Table 1.

From Table 1, we observe that as the number of rays increases to 1000 rings, the detector response tends to converge. Hence, in the following simulation, we will utilize 1000 rings of rays.

Table 1 Changes in the number of rays with simulation results (SB-3)

Number	Number of light (rings)	Detector response result
1	100	1.0908e-6
2	200	8.5724e-7
3	500	1.2615e-6
4	600	1.2585e-6
5	700	1.3414e-6
6	800	1.3944e-6
7	1000	1.2962e-6
8	1200	1.2357e-6
9	1500	1.2872e-6

In TracePro, modeling and simulation testing were performed for the multi-element high-precision scatter measurement system mentioned above. Simulation analysis was conducted for various surface characteristics, and the results are displayed in Fig. 5 below.

The simulation results in Fig. 5 show that the detector received 7.8×10^{-4} units of light energy for surface property a, and 1.35×10^{-2} units of light energy for surface property b. It is evident that different surface properties have a notable impact on the scattering characteristics of the component, as the energy received by the detector differs by two orders of magnitude.

At the same point, the surface roughness remains

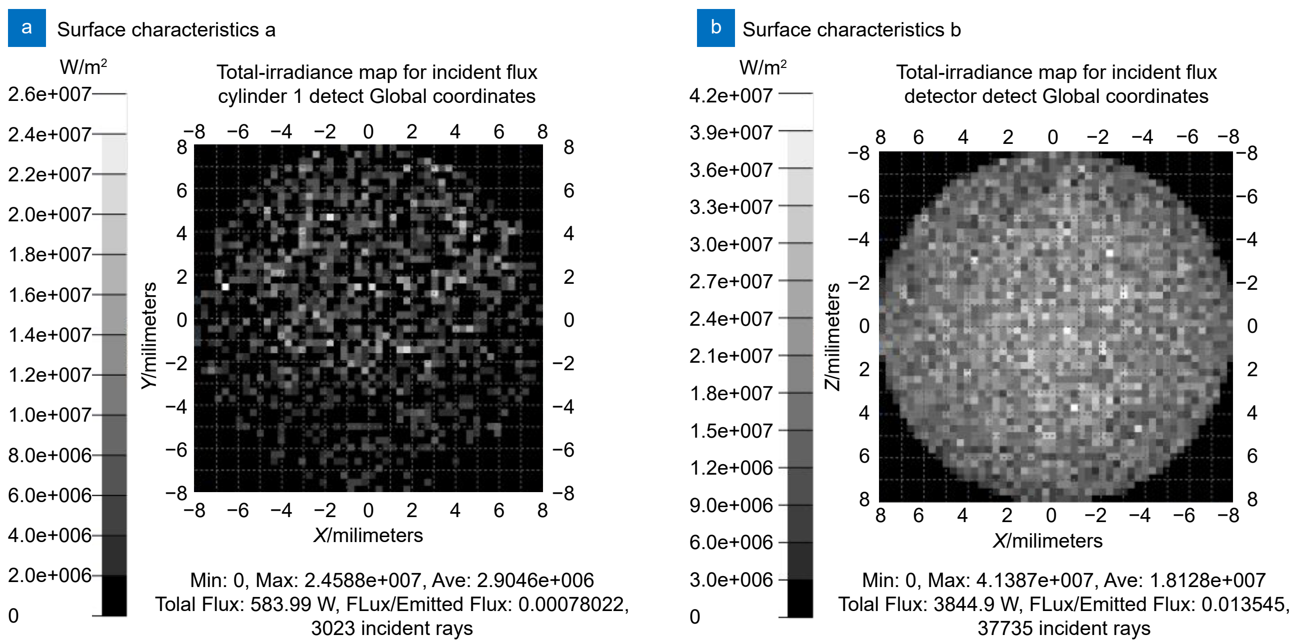

Fig. 5 Simulation results of different surface characteristics

unchanged. The simulation displays results for incident angles θ_i of 15°, 20°, and 30° in Fig. 3.

The data in Fig. 6 indicates that when light is incident at 15°, 20°, and 30°, the detector registers light energy of 0.1022, 0.0993, and 0.0149, respectively. This reveals a substantial variation in the light energy detected by the detector at different incident angles, with differences of up to tenfold. Furthermore, as the incident angle increases, the disparity in detected energy becomes even more pronounced. Hence, it is important to introduce high-precision measurement components to capture the distribution characteristics effectively.

To validate the system's measurement of the TIS characteristics of the material surface, simulations of the TIS on the whiteboard and SB-3 material surfaces were performed, and the results are presented in Table 2.

Prior to usage, the TIS derived from the BSDF of the SB-3 (aluminum-based) material, as measured by the scatterometer, is compared with the TIS directly tested by our system. The fitted curve is depicted in Fig. 7.

From Fig. 7, it is evident that the TIS obtained directly from the system closely aligns with the results obtained through the scatterometer, showing a tendency toward consistency. This suggests that the TIS of the material obtained using this system is accurate and dependable. When the incident angle exceeds 70°, a sudden change is observed in the TIS value. Why does this happen? This will be the focus of our next study.

Conclusion

Space telescopes are crucial for accurate astronomical observations, and their performance depends on the light-suppression material used. This material plays a key role in suppressing scattered light. A high-precision scattered light distribution measurement system has been designed based on the principle of scattered light detection,

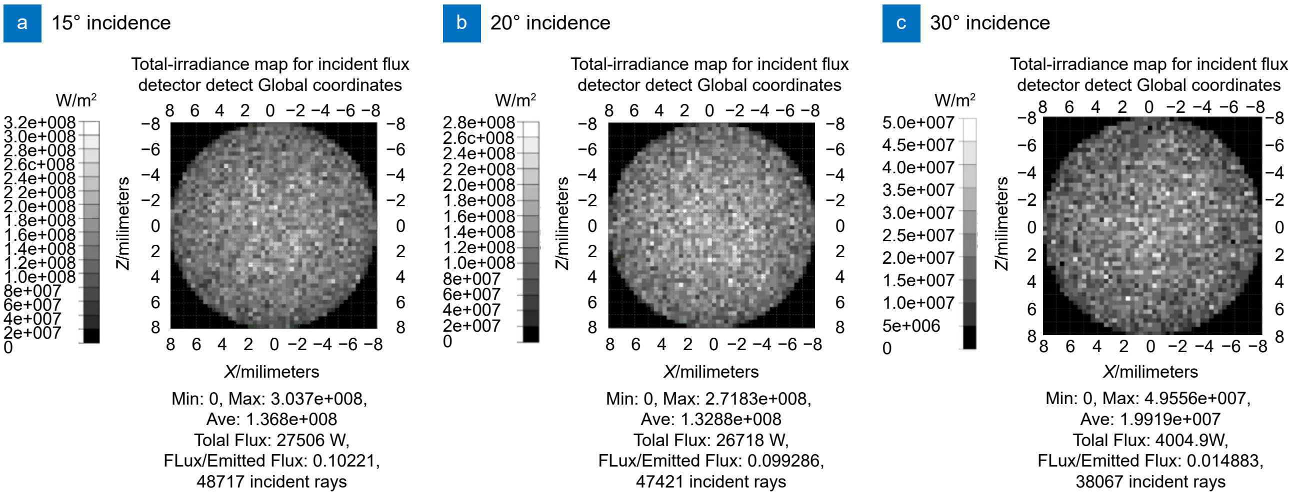

Fig. 6 Simulation results of different incident angles

Table 2 Simulation results of TIS characteristics of material surface

Incident angle	Whiteboard	SB-3	TIS
6°	1.0779e-4	1.2962e-6	0.01203
20°	9.8612e-5	1.2853e-6	0.01303
40°	1.0406e-4	1.4725e-6	0.01415
60°	9.7901e-5	2.317e-6	0.02366

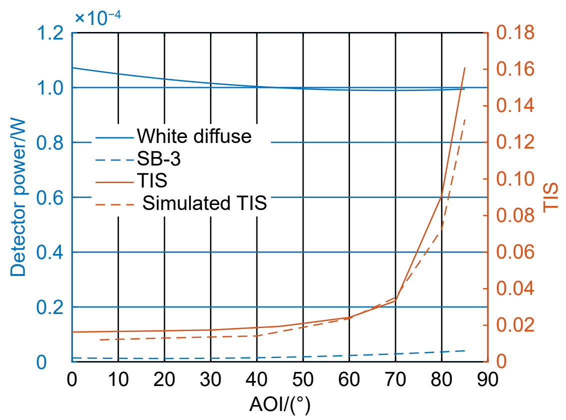

Fig. 7 TIS result comparison

analysis of measurement systems, and practical detection experience. Modeling and simulation have revealed that surface roughness and angle of incidence significantly impact scattered light distribution, with nonlinear changes in different materials. Accurate measurement of scattered light characteristics is essential for cutting-edge design. Materials possess varying degrees of surface non-uniformity and roughness, contingent upon their surface characteristics. In the realm of optical components, roughness induces multiple scattering of incident on the surface, thereby elevating the Total Integrated Scattering value of the material. The extent of this scattering phenomenon is directly proportional to the roughness of the surface. Consequently, the selection of materials with specific surface characteristics becomes imperative in designing optical components for particular purposes. For instance, optimizing the light absorption performance of a light shield can be achieved by considering the relationship between TIS and surface roughness of the material. Moreover, for certain optical components, measures are implemented to mitigate the scattering loss originating from roughness by acknowledging its impact on the Total Integrated Scattering. The total integrated scattering tends to increase with the angle of incidence for various incident light angles. When the angle of incidence is within a small range (⩽30°), the increase in TIS becomes less significant. However, for angles of incidence >30°, TIS shows a more pronounced increase. Notably, when the angle of incidence exceeds 70°, a sudden jump in TIS values occurs. Investigating the cause of this phenomenon will be the focus of our future research.

Integrally studying scattered light characteristics provides a scientific basis for optimizing space telescope design, understanding the impact mechanism of light suppression materials, developing new materials, improving measurement methods and data simulation techniques, and improving the observation accuracy and performance. This study also serves as a reference for stray light suppression, high-performance optical instrument development, and computational optics research.

利益冲突: 所有作者声明无利益冲突

参考文献

[1] Wang X Y, Bai S J, Zhang Q, et al. Research progress of telescopes for space-based gravitational wave missions[J]. *Opto-Electron Eng*, 2023, **50**(11): 230219.
王小勇, 白绍竣, 张倩, 等. 空间引力波探测望远镜研究进展[J]. 光电工程, 2023, **50**(11): 230219.

[2] Zhang Y H, Zhong Z Q, Zhang B. Analysis of surface scattering characteristics of ultra-smooth optical components in gravitational wave detection system[J]. *Opto-Electron Eng*, 2023, **50**(11): 230222.
张耘豪, 钟哲强, 张彬. 空间引力波探测系统中超光滑光学元件表面散射特性分析[J]. 光电工程, 2023, **50**(11): 230222.

[3] Detrio J A, Miner S M. Standardized total integrated scatter measurements of optical surfaces[J]. *Opt Eng*, 1985, **24**(3): 243419.

[4] Chen Y S. A method for measuring the total integrated scattering from laser mirrors[J]. *Acta Opt Sin*, 1984, **4**(3): 285−288.
陈奕升. 一种测量激光反射镜总积分散射的方法[J]. 光学学报, 1984, **4**(3): 285−288.

[5] Stover J C. *Optical Scattering: Measurement and Analysis*[M]. New York: McGraw-Hill, 1990.

[6] Grochocki F, Fleming J. Stray light testing of the OLI telescope[J]. *Proc SPIE*, 2010, **7794**: 77940W.

[7] Liebe C C, Scherr L M. Sun-induced veiling glare in dusty camera optics[J]. *Opt Eng*, 2004, **43**(2): 493−499.

[8] Peterson G L. Stray light test station for measuring point source transmission and thermal background of visible and infrared sensors[J]. *Proc SPIE*, 2008, **7069**: 70690M.

[9] Fest E C. *Stray Light Analysis and Control*[M]. Bellingham: SPIE, 2013.

[10] Liao Z B, Jiao W C, Fu R M. Veiling glare index calculation for refract optical system[J]. *Acta Photonica Sin*, 2011, **40**(3): 424.

[11] Coppens J, Franssen L, van den Berg T J T P. Reliability of the compensation comparison method for measuring retinal stray light studied using Monte-Carlo simulations[J]. *J Biomed Opt*, 2006, **11**(5): 054010.

[12] Dittman M G, Donley E, Grochocki F. Deterministic sequential stray light analysis[J]. *Proc SPIE*, 2010, **7794**: 77940T.

[13] Ashikhmin M, Shirley P. An anisotropic phong BRDF model[J]. *J Graphics Tools*, 2000, **5**(2): 25−32.

[14] Schlick C. An inexpensive BRDF model for physically-based rendering[J]. *Computer Graphics Forum*, 1994, **13**(3): 233−246.

[15] Snyder W C, Wan Z M. BRDF models to predict spectral reflectance and emissivity in the thermal infrared[J]. *IEEE Trans Geosci Remote Sens*, 1998, **36**(1): 214−225.

[16] Lawrence J, Rusinkiewicz S, Ramamoorthi R. Efficient BRDF importance sampling using a factored representation[J]. *ACM Trans Graphics*, 2004, **23**(3): 496−505.

[17] Boynton P A, Kelley E F. Stray light compensation in small area contrast measurements of projection displays[J]. *Proc SPIE*, 2002, **4657**: 122−130.

[18] Zhong X, Jia J Q. Stray light removing design and simulation of spaceborne camera[J]. *Opt Precis Eng*, 2009, **17**(3): 621−625.
钟兴, 贾继强. 空间相机消杂光设计及仿真[J]. 光学 精密工程,

2009, **17**(3): 621−625.

[19] Leviton D B, Gardner L D, Fineschi S, et al. White-light stray light test of the SOHO UVCS[J]. *Proc SPIE*, 1998, **3443**: 50−60.

[20] Fleming J, Grochocki F, Finch T, et al. New stray light test facility and initial results[J]. *Proc SPIE*, 2008, **7069**: 70690O.

[21] Blarre L, Mestreau A. Stray light characterization of optical systems[J]. *Proc SPIE*, 1996, **2775**: 279−286.

[22] General Administration of Quality Supervision, Inspection and Quarantine of the People's Republic of China, Standardization Administration of the People's Republic of China. Veiling glare of optical systems-methods of measurement: GB/T 10988–2009[S]. Beijing: Standards Press of China, 2009.

中华人民共和国国家质量监督检验检疫总局, 中国国家标准化管理委员会. 光学系统杂(散)光测量方法: GB/T 10988–2009[S]. 北京: 中国标准出版社, 2009.

作者简介

【通信作者】刘巍 (1990-)，男，中国科学院西安光学精密机械研究所工程师。2015 年获得北京理工大学硕士学位。主要从事极弱目标模拟与探测、精密光电测量仪器、杂散光测试及仿真技术等方面的研究，发表学术论文、专利 20 余篇。

E-mail: liuwei1@opt.ac.cn

扫描二维码，获取PDF全文

Research on integrated scattering characteristics of extinctive materials for spaceborne telescopes

Liu Wei[1*], Li Zhaohui[1], Mao Zhen[1,2], Zhao Jianke[1], Zhu Hui[1], Wei Ziwei[1], Liu Yong[1], Yin Yunfei[1]

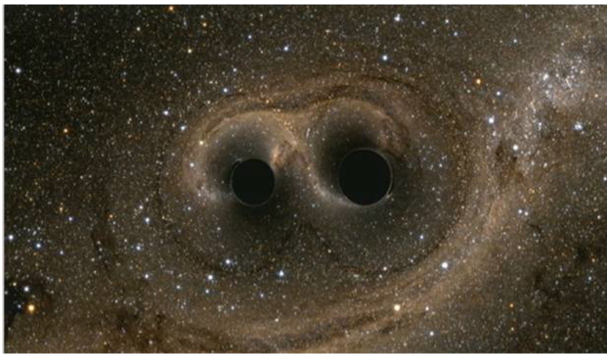

Gravitational wave detection

Overview: Gravitational wave detection is a prominent and highly anticipated research area in modern science. With technological advancements and the development of scientific theories, our understanding of the techniques and methods for detecting gravitational waves has deepened. Gravitational waves are disturbances predicted by Einstein's general theory of relativity, arising from the curvature of spacetime caused by mass and energy. The detection of gravitational waves holds significant importance in comprehending the evolution of the universe, black hole physics, and the origin of the cosmos, among other scientific inquiries. However, due to the extraordinarily weak intensity of gravitational waves, detection necessitates high-precision measurement devices and sophisticated technical means.

As one of the key tools for detecting gravitational waves, space-based telescopes offer advantages such as high precision, high resolution, and the ability to conduct long-duration observations. However, these telescopes encounter interference during observations, including cosmic background and scattered light generated by the telescope itself. To these interferences, extinguishing materials are used to reduce scattered light. These materials possess the ability to absorb or scatter light, effectively minimizing light reflection and scattering and thereby enhancing observation accuracy and signal-to-noise ratio of telescopes. In order to gain a better understanding of the scattering characteristics of extinguishing materials, this study analyzes and examines the design features of scattering light measurement systems both domestically and internationally, building upon the foundations of scattering theory. By combining practical detection challenges and experiences, a test device for assessing the integral scattering characteristics of extinguishing materials employed in space-based telescopes is devised, facilitating more comprehensive measurements of their scattering characteristics. Through simulation modeling and comparisons with actual measurements, it is concluded that the surface roughness of components and the incident angle of light impact the distribution of component scattering, especially in different materials where scattering characteristics demonstrate changes with increasing incident angles. Consequently, achieving precise measurements of the scattering characteristics distribution of components holds paramount importance in cutting-edge design endeavors. This research provides a more comprehensive and accurate understanding of the distribution of scattering characteristics based on the specific properties of extinguishing materials, serving as a valuable reference for stray light measurement and suppression, development and calibration of high-performance optical instruments, and research within the field of computational optics, among others. Ultimately, it establishes a foundation for material selection, characteristic exploration, stray light analysis, and suppression in the context of space-based gravitational wave detection telescopes.

Liu W, Li Z H, Mao Z, et al. Research on integrated scattering characteristics of extinctive materials for spaceborne telescopes[J]. *Opto-Electron Eng*, 2024, **51**(2): 230206; DOI: 10.12086/oee.2024.230206

Foundation item: Project supported by National Key Research and Development Plan (2021YFC2202203)

[1]Xi'an Institute of Optics and Precision Mechanics, Chinese Academy of Sciences, Xi'an, Shaanxi 710119, China; [2]University of Chinese Academy of Sciences, Beijing 100049, China

* E-mail: liuwei1@opt.ac.cn